# Robotic Simulation of Flexible-Body Spacecraft Dynamics

Justin C. Brannan[1] and Craig R. Carignan[2]

***Abstract*— A robotic testbed has been developed to conduct hardware-in-the-loop simulations of a robotic servicer interacting with a client satellite on-orbit. By creating an analytical model of a satellite with flexible appendages, it is possible to simulate the system response to external force and torque inputs and compare the predicted system motion to a robot mass simulator outfitted with physical appendages. This validation effort includes multiple test cases that encompass the types of interaction forces a satellite might experience during a nominal on-orbit servicing mission and aims to show the simulation's ability to capture the physical system response. After incorporating the flexible-body dynamics into the robotic mass simulator at NASA Goddard Space Flight Center (GSFC), a hardware-in-the-loop simulation can be used to characterize the potential impact of structural flexibility on an end-to-end satellite servicing mission.**

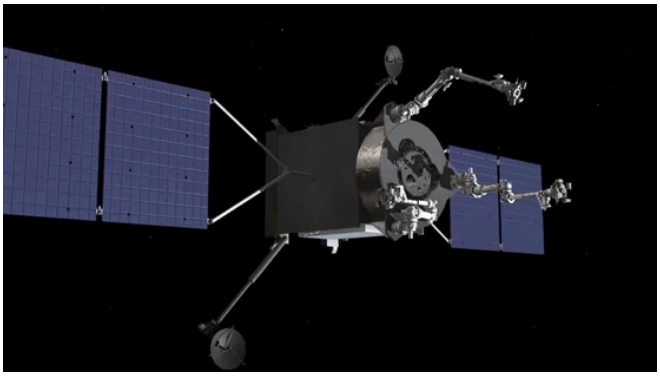

Fig. 1. Example rendering of a robotic servicing vehicle concept.

## I. INTRODUCTION

SATELLITE failures that once led to end-of-life may eventually be addressed using robotic servicing platforms. To achieve such a goal, it is critical that ground simulations be developed to advance the state-of-the-art technologies and test crucial aspects of a servicing mission. This research aims to improve the current ground-based dynamic simulation capabilities by developing a flexible-body simulation of a client satellite interacting with a robotic servicing vehicle. This is the first time the flexible-body dynamics of a free-flying spacecraft has been simulated on a robot. Additionally, this research includes a validation of the coupled dynamics by showing the real flexible hardware on a hardware-in-the-loop simulated satellite hub and comparing the physical response to that of the developed model.

A strong economic incentive exists due to the cost of losing critical assets such as communication satellite services, which can potentially cost millions of dollars per day. In a more general sense, working towards overcoming failures such as the depletion of fuel can lead to expanding a satellite's end-of-life, which has the potential to offset the costs of developing multi-million dollar follow-on spacecraft. NASA's Robotic Refueling Mission (RRM), currently taking place on the International Space Station, is one example demonstration of this technology, and might help enable the development of a robotic servicing vehicle such as that shown in Fig. 1.

Many other organizations and agencies are realizing the potential benefits of robotic servicing missions, such as drastically reducing the total cost of future endeavors and increasing both the reliability and safety of access to space. Other example on-orbit demonstrations include Japan's National Space Development Agency (NASDA) Engineering Test Satellite No. 7 (ETS-VII) and the United States Defense Advanced Research Projects Agency (DARPA) Orbital Express satellite.

The Orbital Express mission proved to be a crucial leap in terms of proving the guidance, navigation and control capabilities on-orbit, and much of its success was attributed to the availability of ground-based testbeds, used to develop and test various aspects of the overall mission [6]. One type of these motion-based platforms includes using commercial robot manipulators to emulate the six degree-of-freedom rigid body motion of a target and chaser spacecraft. For example, the Japanese Aerospace Exploration Agency (JAXA) developed a ground simulator consisting of a pair of Mitsubishi PA-10 robots to study the contact dynamics involved during the insertion of a capture probe into the thruster nozzle of a satellite [12]. Chinese investigators also developed a real-time simulation system to emulate the capturing process in 3D space, using a pair of GRB3016 industrial robots [11]. More recently, the German Aerospace Center (DLR) and the U.S. Naval Research Laboratory have each developed a hardware-in-the-loop system for simulating proximity operations of on-orbit servicing missions, using a pair of robots mounted on a rail and/or gantry system, to simulate the relative motion between a chaser and target spacecraft [1], [2], [7].

In a similar effort, the Satellite Servicing Capabilities Office at NASA Goddard Space Flight Center has developed a ground-based testbed, where robots are used to mimic the "free-floating" rigid-body dynamics of a given satellite of interest. As part of this testbed, various client satellite mockups are attached to the Rotopod robotic demonstration

[1]J. Brannan is an aerospace engineer with Emergent Space Technologies, Greenbelt, Maryland justin.brannan@emergentspace.com

[2]C. Carignan is a research associate professor with the Space Systems Laboratory, University of Maryland, College Park Maryland craigc@ssl.umd.edu

unit, as seen in Fig. 2.

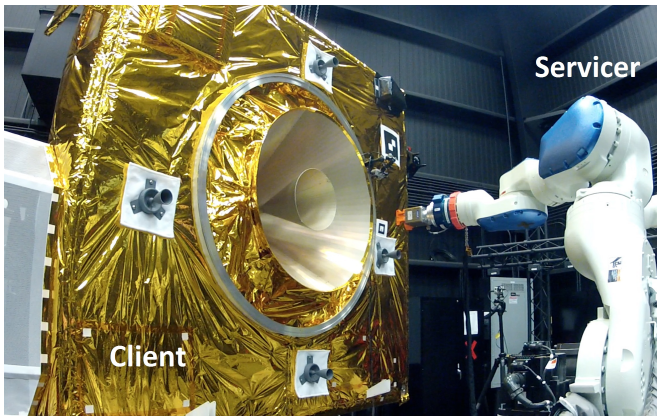


Fig. 2. Example testbed using Rotopod and Motoman SIA-50 robotic demonstration units to simulate the dynamics of a client and servicing spacecraft, respectively.

Note how each of these platforms have only portrayed the rigid body dynamics of a spacecraft, mostly due to the size, flexibility, and cost of adding large solar panels, booms and antennae to the given robotic platform. This imposes an unnecessary limit to the simulation's fidelity, since the initial contact and ensuing servicing tasks have the potential to excite the modes of the appendages. For this reason, it is necessary to artificially add the flexible-body dynamics to study how to mitigate any damage to the client satellite that might be caused by various flexible appendages and render servicing tasks infeasible. Examples of this undesired excitation were documented during the deployment of appendages on-orbit [10], and were predicted during initial testing of Langley's Large Hoop Antenna [5].

As future spacecraft continue to increase in complexity, it is imperative that improvements be made to ground-based simulation capabilities, including the interaction between various flexible-body spacecraft to ensure that various on-orbit servicing tasks can be controlled in a manner that will neither damage the client satellite nor cause instability in the robotic control system. The proposed solution is to model the dominant modes of a given satellite system and incorporate the flexible-body model of an on-orbit satellite to simulate the system response on a real-time robotic testbed.

The organization of the paper is as follows. The flexible-body satellite dynamics used to model the spacecraft system are provided in Section 2. Section 3 describes a hardware-in-the-loop validation effort, utilizing a Motoman SIA10D robot to simulate the flexible-body dynamics of a physical appendage, and final conclusions and future work are discussed in Section 4.

## II. Development of Satellite Dynamics

Although the study of flexible-body dynamics on-orbit has been pursued for decades, the primary concern has only been how to control the spacecraft attitude. For the application of robotic satellite servicing, it is necessary to expand on this knowledge, since even minor disturbances in displacement can mean the difference between a successful docking/capture or an impact and potential loss of contact.

The dynamics developed in this research are based on Shabana and Schiavo's derivation of the dynamic equations of motion of a general flexible-body [9], [8]. Commercial software packages such as Modelica$^{TM}$ are built upon these coupled dynamics, but are not implementable on a real-time testbed. In the pursuit of this goal, the proposed research develops a reduced-order model of the coupled dynamics to conduct hardware-in-the-loop simulations. The result of these simulations will be used to assess the impact of flexible-body excitation on a robotic servicing mission.

### A. Equations of Motion

The flexible-body equations of motion describing the motion of a spacecraft with flexible appendages will now be derived.

Let $x^T = \left[R^T \theta^T q_f^T\right]$ represent the combined flexible-body state of a satellite, where $R$ is the rigid body position of the hub, $\theta$ is the rigid body orientation of the hub, and $q_f$ is the modal position of the satellite appendage(s). The external input profile is represented in the satellite frame by $\left[\bar{u}_{input}^T\right] = \left[\bar{F}_{ext}^T \bar{T}_{ext}^T \bar{Q}_{ext}^T\right]$, which includes the forces ($\bar{F}_{ext}$, $\bar{Q}_{ext}$) and torques ($\bar{T}_{ext}$) experienced from the initial contact of a servicing satellite.

By using the principle of virtual work, the flexible-body equations of motion can be derived to evaluate the resulting motion of the satellite due to interaction forces from a robotic servicing vehicle:

$$[M_{system}]\,[\ddot{\bar{x}}] = [Q_{system}] + [\bar{u}_{input}] \tag{1}$$

with the inertia matrix, $M_{system}$, of a satellite hub with two flexible appendages given by:

$$M_{system} = \begin{bmatrix} M_{RR} & M_{R\theta} & \bar{S}_1 & \bar{S}_2 \\ M_{R\theta}{}^T & M_{\theta\theta} & \bar{I}_{\theta f1} & \bar{I}_{\theta f2} \\ \bar{S}_1{}^T & \bar{I}_{\theta f1}{}^T & m_{ff1} & 0_{nxn} \\ \bar{S}_2{}^T & \bar{I}_{\theta f2}{}^T & 0_{nxn} & m_{ff2} \end{bmatrix} \tag{2}$$

$$M_{RR} = m_s I_{3x3} + m_{RR_1} + m_{RR_2} \tag{3}$$

$$M_{R\theta} = m_s \tilde{\bar{r}}_{cm_s}^T + \tilde{\bar{S}}_{t_1}^T + \tilde{\bar{S}}_{t_2}^T \tag{4}$$

$$M_{\theta\theta} = I_{o_s} + \bar{I}_{\theta\theta_1} + \bar{I}_{\theta\theta_2} \tag{5}$$

where $m_s$ is the mass of the satellite hub, $I_{3x3}$ is an identity matrix, $\tilde{\bar{r}}_{cm_s}$ is the skew-symmetric form of the center of mass of the satellite hub expressed in body coordinates, and $\bar{S}$, $\bar{I}_{\theta f}$, $m_{ff}$, $m_{RR}$, $\tilde{\bar{S}}_t$, and $\bar{I}_{\theta\theta}$ represent modal integrals defined in [4].

The acceleration of the system is given by $\ddot{\bar{x}}$, which includes translational, rotational and modal contributions to the overall system motion:

$$[\ddot{\bar{x}}] = \begin{bmatrix} \ddot{\bar{R}} \\ \bar{\alpha} \\ \ddot{q}_f \end{bmatrix} \tag{6}$$

and the quadratic velocity vector, $Q_{system}$, includes the Coriolis/centripetal force terms, given by

$$Q_{system} = \begin{bmatrix} m_s\tilde{\omega}_s\left(\tilde{\omega}_s\bar{r}_{cm_s}\right) + Q^R_{v_1} + Q^R_{v_2} \\ \tilde{\omega}_s I_{o_s}\omega_s + Q^\theta_{v_1} + Q^\theta_{v_2} \\ Q^f_{v_1} - k_{ff_1}q_{f_1} - b_{ff_1}\dot{q}_{f_1} \\ Q^f_{v_2} - k_{ff_2}q_{f_2} - b_{ff_2}\dot{q}_{f_2} \end{bmatrix} \tag{7}$$

where $\tilde{\omega}$ is the skew-symmetric form of the rotational velocity of the satellite hub, the stiffness and damping properties of the flexible body are given by $k_{ff}$ and $b_{ff}$, respectively and ${Q_v}^R$, ${Q_v}^\theta$, and ${Q_v}^f$ are quadratic velocity terms also defined in [4].

It is important to note that although (2) and (7) are given for a particular satellite configuration where only two appendages are attached, the methods described are easily expanded to include an arbitrary number of appendages, each described by a sufficient number of modes that can accurately capture the necessary dynamics of the given system. Discussion regarding how to determine a sufficient number of modes to include for a given appendage is given in [4], however this is heavily dependent on the type of appendage being described. For the example system used throughout this article, it is assumed that: (a) each appendage can be accurately represented by a Euler-Bernoulli beam; (b) the dominant response of the system can be captured using only the first few modes; and (c) each appendage can be approximated as having a single flexible degree-of-freedom.

Once the system mass matrix and quadratic velocity vector are derived for a given system, the system dynamics in (1) can be propagated over time by solving for the accelerations $\ddot{\bar{x}}$ and integrating the result using a fourth order Runge-Kutta method.

## III. Hardware-in-the-Loop Validation Effort

Since the final goal of this research is to incorporate the flexible-body satellite model into a real-time, hardware-in-the-loop simulation, a validation effort was conducted utilizing a robotic demonstration testbed located at NASA Goddard Space Flight Center (GSFC). This effort includes a comprehensive example demonstrating how a simulation of the coupled rigid- and flexible-body dynamics can be used to predict the motion of a physical system.

### A. Robotic Mass Simulation Test Setup

This end-to-end validation effort involves a Motoman SIA10D robot outfitted with two flexible appendages, as seen in Fig. 3. By conducting a hardware-in-the-loop simulation, real-time force and torque profiles can be input to the system, where the robot acts as a satellite mass simulator that can interact with the servicer. Although the robot is only acting like a rigid-body, the sensed interaction forces due to the appendage motion feed into the simulation and create a coupled rigid- and flexible-body system response.

The simulation setup is illustrated in Fig. 4, where the combined external input and flexible appendage motion is measured by a force/torque sensor located between the robot flange and physical appendages. The measured forces

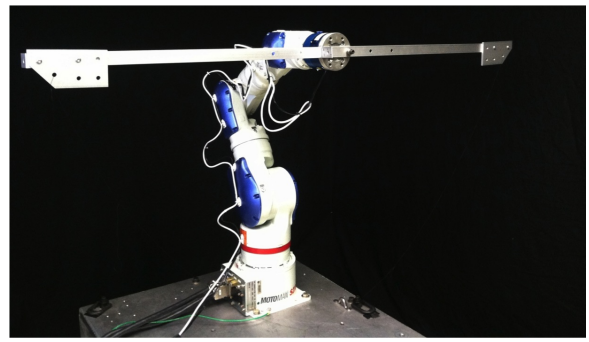

Fig. 3. Motoman SIA10D robot with physical appendages attached.

resulting from the oscillatory motion of the appendages are input to the rigid-body dynamics script which predicts the response of the satellite system. This predicted motion is tracked by the robot, which is continuously influenced by the appendage oscillations in real-time.

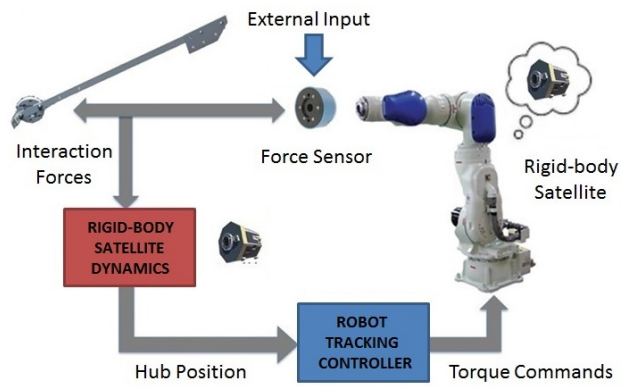


Fig. 4. Diagram of rigid-body simulation with physical appendages.

A more detailed block diagram is shown in Fig. 5 to include a more conventional portrayal of system input and output. The sensed forces from both the external input profile and the induced appendage motion are read into the sensor component, which also converts the force from sensor frame (W) to satellite frame (S). This force profile is input to the satellite forward dynamics, along with the desired mass parameters that characterize the rigid-body satellite hub: the mass, $m_s$, center of mass position, $r_{cm_s}$, and inertia about the body frame axes, $I_{o_s}$. The output of the forward dynamics is the desired flexible-body satellite state, which is input to the robot component. This includes the Motoman robot inverse kinematics and robot servo controller, which computes the torques that actually drive the hardware. The robot forward kinematics model, also part of the robot component, outputs the realized robot motion, which itself reacts to the flexible modes of the physical appendages.

In order to conduct a simulation of the given physical system, it was necessary to derive the structural parameters for the physical appendages seen in Table I, to be used as input to the flexible-body model. Each appendage is modeled as a cantilever beam fixed to a cube-shaped satellite hub, and

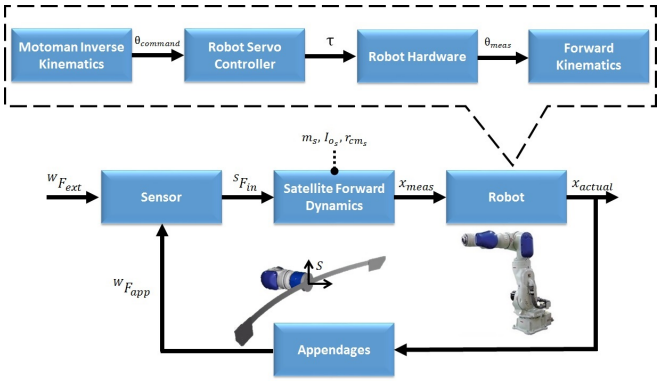


Fig. 5. Block diagram of the interaction between robot and appendages.

the modal displacement is described by an Euler-Bernoulli beam with fixed-free boundary conditions [3]. Note that the modal displacement of each appendage is assumed to only deform about a single axis, and the first two modes of either beam are used to capture the dominant response of the class of flexible-bodies studied in this research. More details about the characterization of the physical appendages are given in [4].

TABLE I

EXAMPLE SATELLITE PARAMETERS USED TO MODEL THE FLEXIBLE-BODY SYSTEM.

| | $m$ (kg) | $L$ (m) | $I_{o_{principal}}$ (kg-m$^2$) | $EI$ (N-m$^2$) | $\zeta$ |
|---|---|---|---|---|---|
| Satellite Hub | 50 | 1 | 8.33, 8.33, 8.33 | - | - |
| Appendage | 0.83 | 0.64 | 9e-3, 2e-5, 9e-3 | 0.46 | 7.2e-3 |

This model is input to the flexible-body dynamics simulation to predict how the actual system responds to various input profiles, where an artificial delay is added to the simulated system response to compensate for the transport delay introduced by the Motoman controller. This enables direct correlation between the measured hardware data and the simulated system response as predicted by the flexible-body dynamics model.

## B. Input Definition

Two test cases were utilized in the validation of the developed flexible-body model, the first of which includes applying a force impulse to the satellite hub to excite the symmetric flexible-body modes, or more specifically the first and third flexible-body system modes. The steady-state response due to this input is shown in Fig. 6, where the two appendages oscillate in unison as the center of mass translates in the direction of the impulse. Similarly, by applying equal and opposite forces to the two appendages, it is possible to excite the asymmetric (second and fourth) flexible-body modes, also shown in Fig. 6.

An exaggerated modal response is accomplished by applying forces directly to the physical appendages. Since the force applied to the appendages is not directly measured, this modal input is approximated as a combination of a rigid-body

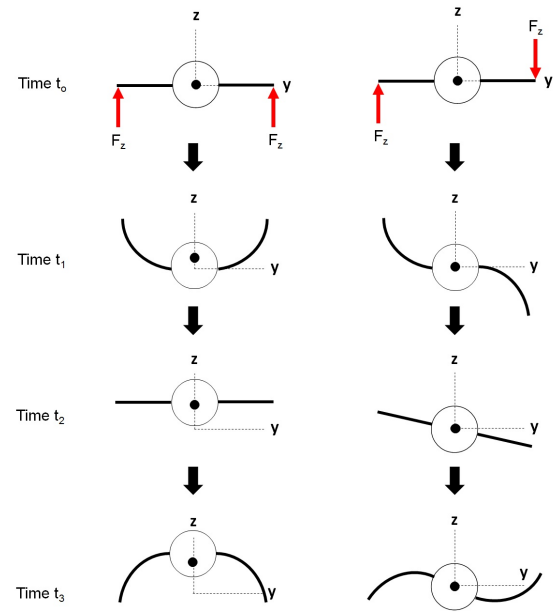


Fig. 6. Initial input and satellite response due to symmetric (left) and asymmetric (right) force impulse applied to the appendages.

excitation and an initial modal position for each appendage, which is valid so long as the deflection occurs before the robot starts moving appreciably. This input profile is then used to drive the simulated flexible-body dynamics, and the resulting motion is compared with the physical system.

## C. Results

*1) Exciting the Symmetric System Modes:* The first example of this coupled dynamics validation effort involves the excitation of symmetric flexible-body modes, and features satellite parameters as described in Table I. The comparison between the physical system and simulated response is shown in Fig. 7, where the net force input produces a constant velocity and the oscillations are due to the excitation of the flexible appendages.

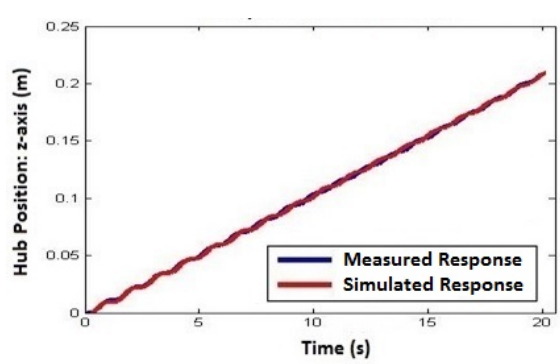


Fig. 7. Simulated and physical system response for 50 kg satellite hub for a symmetric initial deflection of 10 cm.

The error between the predicted and physical flexible-body system response is shown in Fig. 8 to have a maximum magnitude difference of approximately 6 mm, or only about

3% of the total translation. These results also show a beat frequency of 0.028 Hz, which can be explained by the difference in structural rigidity between the two physical appendages, of approximately 0.3 N-m$^2$.

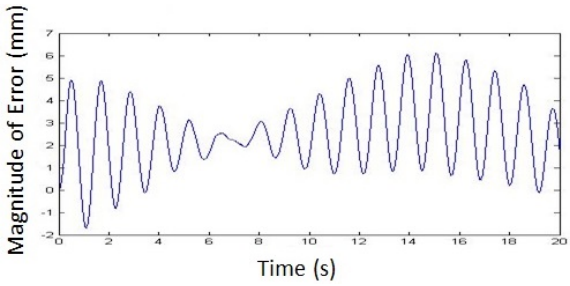


Fig. 8. Hub position error between simulated and physical system symmetric flexible-body response for 50 kg satellite hub.

Another possible source of error is introduced by a small difference in initial modal position between the two appendages, due to the appendages not being pulled with the exact same force. This caused a non-zero torque input in addition to the expected symmetric appendage motion, seen in Fig. 9. As the simulation continues, the oscillation of the two appendages become more asymmetric, causing more energy to go into rotation instead of pure translation.

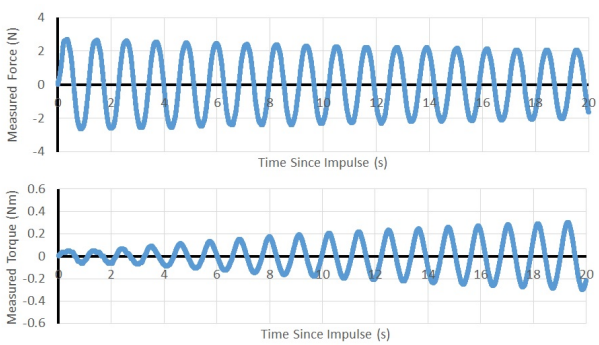


Fig. 9. Measured input profiles for 50 kg satellite hub exhibiting symmetric flexible-body excitation due to an initial force impulse.

Additional examples were produced featuring a smaller (25 kg) and larger (100 kg) mass satellite hub with the same input profile as the previous case. The maximum error was found to be inversely proportional to the satellite hub mass, still resulting in approximately a 3% error between the simulated and physical results in both cases, relative to the total translation over 20 s.

*2) Exciting the Asymmetric System Modes:* To produce the asymmetric motion seen in Fig. 6, the two appendages were pulled with equal and opposite forces. This type of input can be thought of as a combination of an initial modal position and a torque impulse exerted on the satellite hub, resulting in 180° asymmetric appendage motion and a net torque impulse applied to the hub.

Multiple test cases were conducted to feature principle inertias of 41.7 kg-m$^2$, 16.7 kg-m$^2$, and 8.3 kg-m$^2$, corresponding to a 250 kg, 100 kg, and 50 kg cube-shaped satellite hub, respectively. Figs. 10 and 11 show how the physical, measured system data compares to the simulated, predicted response, with a maximum error of only 0.2°, or about 6% of the total rotation over the ten second simulation.

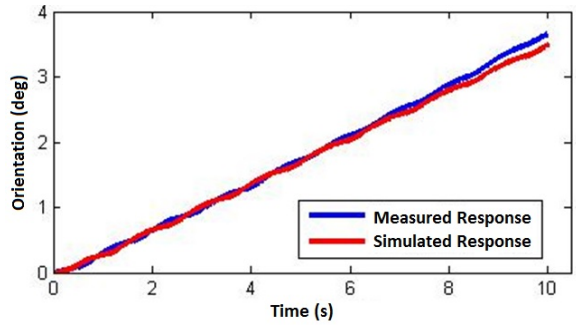


Fig. 10. Simulated and physical system response for 250 kg satellite hub for an asymmetric initial deflection of 8 cm.

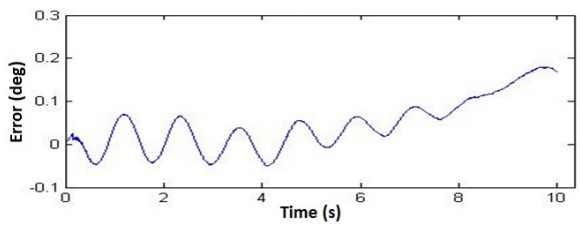


Fig. 11. Hub position error between simulated and physical system asymmetric flexible-body response for 250 kg satellite hub.

Similar to the symmetric flexible-body response, there is a frequency discrepancy that is attributed to a lack of symmetry in the applied input profile. In this case, both a slightly imperfect asymmetric excitation and the difference in structural rigidity between the two appendages cause a small frequency shift. Although there is still room for improvement, the small discrepancy recorded shows how the flexible-body simulation is able to capture the dominant response of the physical system for even the more complicated, asymmetric input case.

### *D. Discussion*

The proposed validation effort can be achieved in two steps, where it must first be proven that the robot used in the hardware-in-the-loop (HIL) simulation can react as if it were a rigid hub satellite. By using the conservation of momentum to predict the amplitude of hub motion based on the initial deflection of the appendages, it is possible to check if the robot in the hardware-in-the-loop simulation agrees with a theoretical rigid hub satellite. This is shown in Table II, where three separate satellite systems are compared for a symmetric set of initial modal conditions. A similar comparison is shown in Table III for the asymmetric sets of initial modal conditions, where the two appendages were initially pulled a distance, $qf_{IC}$, in opposite directions.

In each of these cases, it is clear that the theoretical and measured amplitude of satellite hub motion is comparable, with minor error attributed to limited robot control bandwidth

TABLE II

COMPARISON OF THEORETICAL, MEASURED AND SIMULATED SATELLITE RESPONSE DUE TO A SYMMETRIC INPUT.

| | | Theoretical | | Measured | | Simulated | |
|---|---|---|---|---|---|---|---|
| $m_s$ | $qf_{IC}$ | Amp | Freq | Amp | Freq | Amp | Freq |
| (kg) | (mm) | (mm) | (Hz) | (mm) | (Hz) | (mm) | (Hz) |
| 25 | 91.3 | 3.9 | 0.828 | 3.5 | 0.880 | 4.4 | 0.839 |
| 50 | 91.3 | 2.0 | 0.825 | 1.9 | 0.881 | 2.3 | 0.831 |
| 100 | 98.4 | 1.1 | 0.824 | 0.9 | 0.883 | 1.2 | 0.827 |

TABLE III

COMPARISON OF THEORETICAL, MEASURED AND SIMULATED SATELLITE RESPONSE DUE TO AN ASYMMETRIC INPUT.

| | | Theoretical | | Measured | | Simulated | |
|---|---|---|---|---|---|---|---|
| $m_s$ | $qf_{IC}$ | Amp | Freq | Amp | Freq | Amp | Freq |
| (kg) | (mm) | (deg) | (Hz) | (deg) | (Hz) | (deg) | (Hz) |
| 50 | 36 | 0.053 | 0.824 | - | - | - | - |
| 100 | 35 | 0.026 | 0.823 | 0.033 | 0.892 | 0.035 | 0.825 |
| 250 | 38.1 | 0.011 | 0.822 | 0.019 | 0.880 | 0.019 | 0.823 |

(about 2-3 Hz), transport delay in the robot controller, and inaccurate or unsynchronized force/torque measurements. Unfortunately, since a significantly large hub-to-appendage mass ratio was utilized during all of the hardware-in-the-loop simulations, the system response frequency did not differ much between the three test cases. The error between theoretical and measured frequencies is in large part due to the estimation of initial modal conditions and the higher-order dynamics characteristic of the physical appendages.

The second step includes directly comparing the simulated system response to the physical, measured system response to determine how accurately the physical system response can be captured, for various satellite systems. This validation also utilizes the comparison of amplitude and frequency shown in Tables II and III as independent descriptions of the system response over time. Note that a hardware-in-the-loop simulation was not conducted for an inertia of 8.3 kg-m$^2$ due to the inability of the robot to react to such small inertias. Due to this limitation, there was no force/torque input profile to input to the simulation.

Although the general trends still match between measured and simulated data, the larger perceived error is attributed to the difficulty of predicting the non-symmetric traits present in the physical hardware and force profile applied to the flexible appendages. This includes non-modeled dynamics such as higher-order modes, errors with the estimation of structural parameters, and the estimation of initial modal conditions. Similar to the previous comparison, the response frequencies do not differ much from the natural frequency of an infinite mass satellite hub, of 0.82 Hz [4]. This suggests that a smaller hub-to-appendage mass ratio should be used in future work, since it is not possible to simulate a smaller mass satellite hub due to the control bandwidth limitations of the Motoman SIA10D robot.

Despite the known sources of error, the presented data suggests that the derived flexible-body dynamics simulation is able to capture the dominant response of a physical system. The described hardware-in-the-loop simulation is thus an accurate emulation of the example simplified on-orbit satellite systems, assuming that the errors presented during this validation effort can be minimized.

## IV. CONCLUSION

The primary goal of this research was to expand on the current literature to develop a robotic simulation of the interaction between a robotic servicer and a flexible-body client spacecraft. A validation of the derived dynamics was conducted utilizing a robotic testbed at NASA GSFC to simulate a physical system. The results from both symmetric and asymmetric test cases have demonstrated how accurately the derived flexible-body model is able to capture the dominant response of a physical system, with sources of error attributed to the physical setup and non-symmetric traits present in the hardware and applied input profile.

This research effort has improved the fidelity of the current robotic demonstration capabilities by adding the flexible-body dynamics to a real-time implementable dynamic simulation and can now be used to assess the impact of flexible-body excitation on a robotic servicing mission. More specifically, the robotic demonstration units at NASA GSFC can now be used to simulate the interaction between a servicing vehicle and client satellite, where the effect of the flexible-body dynamics of either spacecraft can provide insight that may guide the development of mission-level requirements, including approach velocities, satellite servicing procedures, and control algorithms which minimize the effect of excited flexible modes and avoid the possibility of damaging either spacecraft.

## ACKNOWLEDGMENTS

Thanks go to Brian Roberts, Nick Scott, and Stephen Roderick for their support with the flexible-body dynamics implementation. This project was sponsored by the Satellite Servicing Capabilities Office at NASA GSFC under OMES Contract #NNG12CR31C.

## REFERENCES

[1] J. Artigas, M. D. Stefano, W. Rackl, R. Lampariello, B. Brunner, W. Bertleff, R. Burger, O. Porges, A. Giordano, C. Borst, and A. Albu-Schaeffer, "The oos-sim: An on-ground simulation facility for on-orbit servicing robotic operations," in *Proc. of the 2015 IEEE International Conference on Robotics and Automation*, Seattle, May 2015, pp. 2854–2860.

[2] H. Benninghoff, T. Tzschichholz, T. Boge, and T. Rupp, "Hardware-in-the-loop simulation of rendezvous and docking maneuvers in on-orbit servicing missions," in *Proc. of the 28th International Symposium on Space Technology and Science*, Okinawa, June 2011.

[3] R. Blevins, *Formulas for Natural Frequency and Mode Shape*. Krieger Publishing Company, 2001.

[4] J. C. Brannan, "Robotic simulation of flexible-body spacecraft dynamics in a satellite servicing testbed," Master's thesis, University of Maryland, College Park, 2014.

[5] G. Campbell, M. C. Bailey, and W. K. Belvin, "The development of the 15-meter hoop column deployable antenna system with final structural and electromagnetic performance results," *Acta Astronautica*, vol. 17, no. 1, pp. 69–77, 1988.

[6] M. R. Leinz, C.-T. Chen, P. Scott, W. Gaumer, P. Sabasteanski, and M. Beaven, "Modeling, simulation, testing, and verification of the orbital express autonomous rendezvous and capture sensor system (arcss)," in *Society of Photo-Optical Instrumentation Engineers (SPIE) Conference Series*, ser. Society of Photo-Optical Instrumentation Engineers (SPIE) Conference Series, vol. 6958, Apr. 2008, p. 0.

[7] J. Obermark, G. Creamer, B. E. Kelm, W. Wagner, and G. C. Henshaw, "Sumo/frend: vision system for autonomous satellite grapple," in *Proceedings of the SPIE - Sensors and Systems for Space Applications*, vol. 6555, 2007.

[8] F. Schiavo, L. Vigano, and G. Ferretti, "Object-oriented modelling of flexible beams," *Multibody System Dynamics*, vol. 15, pp. 263–286, 2006.

[9] A. A. Shabana, *Dynamics of Multibody Systems, 3rd Ed.* New York: Cambridge University Press, 2005.

[10] J. Sudey, Jr., W. Dellinger, and M. Hagopian, "On-orbit jitter performance of the goes spacecraft and instruments," pp. 664–676, 1996. [Online]. Available: http://dx.doi.org/10.1117/12.254112

[11] W. Xu, B. Liang, Y. Xu, C. Li, and W. Qiang, "A ground experiment system of free-floating robot for capturing space target," *Journal of Intelligent and Robotic systems*, vol. 48, no. 2, pp. 187–208, 2007.

[12] K. Yoshida, H. Nakanishi, H. Ueno, N. Inaba, T. Nishimaki, and M. Oda, "Dynamics, control and impedance matching for robotic capture of a non-cooperative satellite," *Advanced Robotics*, vol. 18, no. 2, pp. 175–198, 2004.